Chemistry – A European Journal

ChemEurJ Chemistry Europe European Chemical Societies Publishing

RESEARCH ARTICLE OPEN ACCESS

Tuning the Twist by Molecular Design: A New Strategy for Hexabenzocoronene-Containing Helical Twistacene

Juan P. Mora-Fuentes[1,2] | Daniel Villar-Castro[1] | J. Francisco Barbosa-de-Bessa[1] | Daniel Aranda[3] | Frank Hampel[2] | Dolores Pérez[1] | M. Eugenia Pérez-Ojeda[2] | Diego Peña[1,4] | Andreas Hirsch[2]

[1]Centro Singular de Investigación de Química Biológica y Materiales Moleculares (CiQUS) and Departamento de Química Orgánica, Universidad De Santiago de Compostela, Santiago de Compostela, Spain | [2]Department of Chemistry and Pharmacy, Institute for Organic Chemistry, Friedrich-Alexander-Universität Erlangen-Nürnberg, Erlangen, Germany | [3]Departamento De Química-Física, Facultad de Ciencias, Universidad De Málaga, Teatinos-Universidad, Málaga, Spain | [4]Oportunius, Galician Innovation Agency (GAIN), Santiago de Compostela, Spain

Correspondence: Juan P. Mora-Fuentes (juanpedro.mora@usc.es) | M. Eugenia Pérez-Ojeda (eugenia.perez-ojeda@fau.de) | Diego Peña (diego.pena@usc.es) | Andreas Hirsch (andreas.hirsch@fau.de)

Received: 8 December 2025 | **Revised:** 9 January 2026 | **Accepted:** 14 January 2026

Keywords: bottom-up approach | nanographenes | scholl reaction | soluble | twistacenes

ABSTRACT

In this work, we present an efficient synthetic methodology that allows precise and selective control on the C–C bonds during the Scholl reaction. The first ever described hexabenzocoronene (HBC)-containing helical twistacene **NG2** has been obtained with very high yield and practically no need for purification, starting from a helical-twisted hexacene **NG1**. X-ray analysis reveals an end-to-end twist angle, from approximately 145° in **NG1** to 132° in **NG2**. This approach has provided access to nanographenes (NGs) with improved properties compared to their planar analogues, in particular, enhanced solubility and high stability. In addition, they exhibit interesting redox properties, which, together with their high molar absorbance and optimal energy levels, highlight their potential as new organic semiconductor materials for emerging photovoltaic and electronic technologies.

1 | Introduction

Recent research in materials field has focused on nanographenes (NGs), that is, structurally extended polycyclic aromatic hydrocarbons (PAHs) with unique electronic, optical, and mechanical properties [1–3]. Among these, hexa-*peri*-hexabenzocoronene (HBC) is considered the smallest and most representative member of the NG family [4–7]. Since the first synthesis of HBC in 1958 by Clar and coworkers [5], several groups have reported alternative procedures to obtain this fascinating structure. [8–19] Among them, the synthetic methodology reported by Mullen et al. based on the cyclotrimerization of diphenylacetylenes followed by oxidative cyclodehydrogenacion (Scholl reaction) had aroused great interest due to its versatility [8], thus allowing the access to new HBC-based NGs.

NGs show promising potential in various applications, including molecular electronics, photonics, energy conversion, chemical sensing, and gas storage [20–24]. The forefront of research aims to utilize organic chemistry to optimize NGs synthesis facing the low processability and the zero band gap of the conventional graphene. However, it is common to observe that NGs exhibit also low processability, which is mainly attributed to the lack of solubility of planar π-system, promoting the formation of aggregates in solution. Additionally, there are some NGs, such as the acene family, that are unstable [25], a factor that leads to a limitation in the lifetime of these materials in potential future applications. In fact, the synthesis of extended NGs is a current challenge as it requires the generation of soluble and stable intermediates, which makes purification, characterization, and processing difficult, thereby limiting the comprehensive exploration of their

fundamental properties. Consequently, improvements in the design of these systems appear crucial to overcome that limitation. Various strategies have been developed to enhance the solubility and stability of larger acenes. Among them, including bulky substituents at specific positions in the aromatic core efficiently improves the solubility allowing the purification and characterization processes. Regarding the stability, increasing the number of Clar's sextet [26] as well as including heteroatoms into the conjugated framework allow the obtention of more stable acene-derived systems [27, 28].

Twistacenes are topologically interesting molecules which can overcome some of these challenges [29–40]. This family of helical twisted PAHs is more soluble compared to their planar counterparts due to their low efficient packing through π-π stacking. In addition, the introduction of torsion in PAHs gives rise to the emergence of new properties, such as chirality [41–46], which has very significant applications in the field of nonlinear optics [47–50]. Pascal and coworkers has studied in detail this family of compounds. In 2004, a pentacene derivative with a 144° twist [36], the most highly twisted PAH prepared until then, was prepared in his research group (Figure 1). In 2012, the group led by Zhang reported the synthesis of a stable nona-twistacene obtained by a retro-Diels–Alder reaction [34]. Later, in 2018, the same group presented the synthesis of a dodeca-twistacene [35]. Both structures used pyrene as the main structural unit (Figure 1). The addition of an extra pyrene unit in the center of the aromatic core induced a twisted angle of 124.7°. As a result, the main skeleton of the compound does not exhibit good planarity and differs significantly from pyrene-containing nitrogen-doped NGs [28] becoming the longest twistacene synthesized to date. However, it was at the beginning of 2018, when Kilway and coworkers reported the most distorted twistacene, with an end-to-end torsion angle of 184° [32], making it the widest recorded torsion angle (Figure 1). Hence, two key structural motifs present in these structures are a sterically impeded pyrene moiety (highlighted in blue) and phenanthrene units (highlighted in pink) at the ends of the acene skeleton. Since the photophysical properties depend significantly on the structural variables of the NGs, the combination of both structural motifs is an interesting approach to provide a new perspective in the design of new helical twisted NGs with high chemical stability and great torsion.

In this work, we present the efficient synthesis of the first example of HBC-containing helical twistacene, which features excellent solubility and high stability, fundamental aspects for its integration into optoelectronic devices. In this context, we report the synthesis, complete characterization, and crystal structures of **NG1** and **NG2**, which have an end-to-end twist angle of approximately 145° for **NG1** and 132° for **NG2**. The synthetic strategy involves a sequence of two Diels-Alder cycloadditions based on aryne chemistry and Scholl reaction. Together, this molecular approach not only synergistically integrates helical distortion with aromatic flatness in a single architecture but also opens the door to the development of new materials with highly sophisticated electronic, optical, redox, and self-assembly properties, with great potential for applications in nanotechnology and advanced optoelectronics.

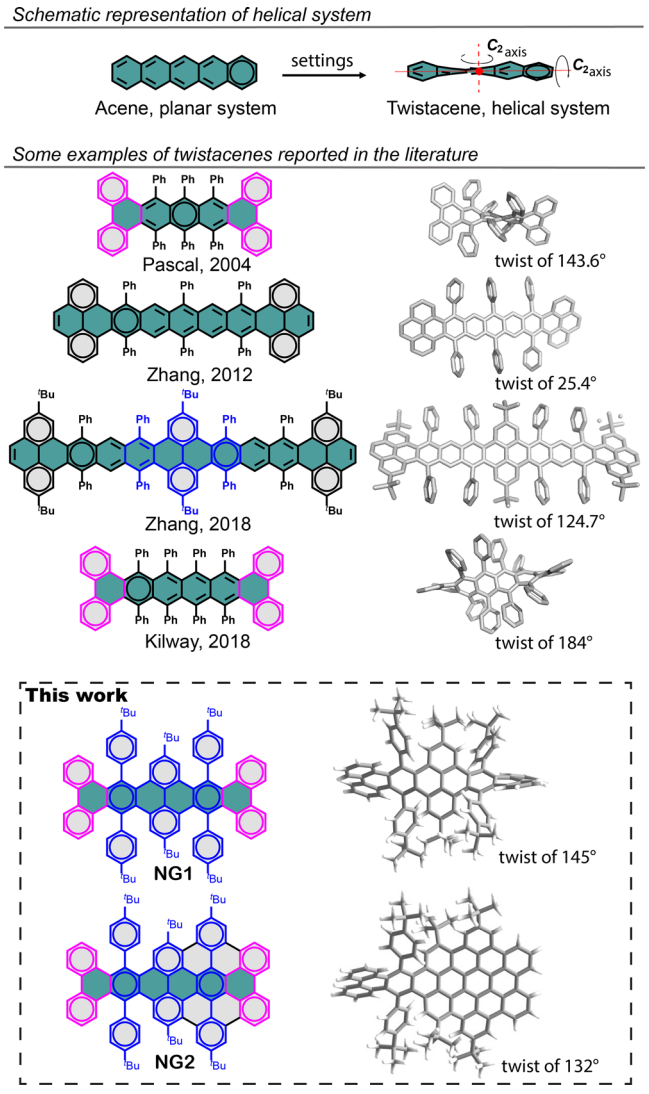

FIGURE 1 | Schematic representation of helical system. Selected previous examples of *twistacenes*. Newly synthesized helically twisted NGs together with their crystal structures.

2 | Results and Discussion

The synthesis of **NG1** and **NG2** is shown in Scheme 1. To synthesize **NG1** through an AB-type Diels Alder reaction, a synthesis of the initial substrates as compound was necessary. **A** [51] and **B1** [52] were prepared from commercially available compounds, respectively, reported in the literature. The first one was prepared via a double Knoevenagel condensation between a tetra-oxidated pyrene unit substituted with ^{t}Bu groups and a propanone derivative [53]. Meanwhile, the latter, compound **B1**, is an aryne precursor already well described in previous works of our research group. Our wide experience in aryne's chemistry prompted us to study the reaction of phenantryne **B1** with the biscyclopentadienone **A**. In this specific case, the DA reaction needs the presence of a fluoride source to generate the aryne in situ, the phenanthryne (**B2**). Following well-known procedures [12], phenantryne precursor **B1** was treated with CsF in presence of A at 60°C for 16 h. Subsequently, the mixture was further

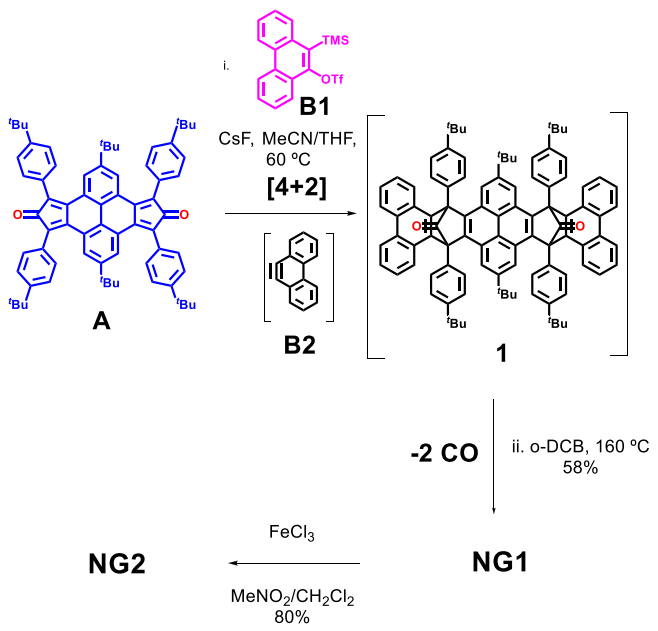

SCHEME 1 | Synthesis of **NG1** and **NG2**

heated to 160°C to promote the chelotropic extrusion of CO, allowing the obtention of **NG1** in 58%. It is important to note that after the two-fold [4+2] reaction, only the intermediate *trans*-**1** is identified, whose structural characterization was achieved by X-ray diffraction analysis. Finally, the graphitization process (Scholl reaction) was performed using $FeCl_3$ (40 eq) with CH_3NO_2 and conducting the reaction at room temperature for 18 h, satisfactorily produces the desired product, **NG2** in an excellent yield.

Owing to the excellent solubility of both compounds in common organic solvents, we tackled their structural characterization. The ^{1}H NMR spectrum in deuterated tetrachloroethane shows a set of well-defined signals at room temperature for **NG1** and **NG2**, which were assigned using ^{13}C and 2D NMR experiments (Supporting Information, Figures S1–S16), are in agreement with the target structure. It is important to note that, at room temperature, it was not possible to assign all the aromatic **NG2** signals. However, it was necessary to cool the sample to –10°C to observe all the signals in the ^{1}H NMR spectrum clearly (Figure 2 and Supporting Information, Figure S17). This suggests that the structure is not completely rigid and that its dynamic behavior is temperature-dependent.

Additionally, its exact mass for **NG1** (m/z = 1243.687 $[M]^+$) and **NG2** (m/z = 1234.6459 $[M]^+$) were also identified by high-resolution matrix-assisted laser desorption ionization/time-of-flight mass spectrometry (MALDI-TOF). The isotopic distribution obtained is consistent with the calculated one, supporting the proposed structure (Supporting Information, Figures S18–S21).

The crystallization process represented a crucial step in assessing reaction conditions. Thanks to the crystal of the intermediate precursor **1**, we realized the Diels-Alder reaction required a higher temperature in order to obtain the desired product. The crystal structure of intermediate precursor **1** was confirmed through X-ray analysis of the crystals grown by slow diffusion of

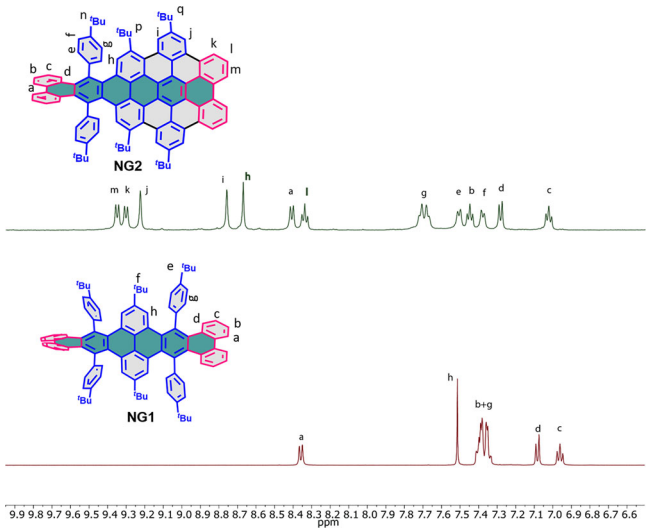

FIGURE 2 | ^{1}H NMR (600 MHz, $CD_2CD_2Cl_4$ at –10 °C) spectra of **NG1** (bottom) and **NG2** (top).

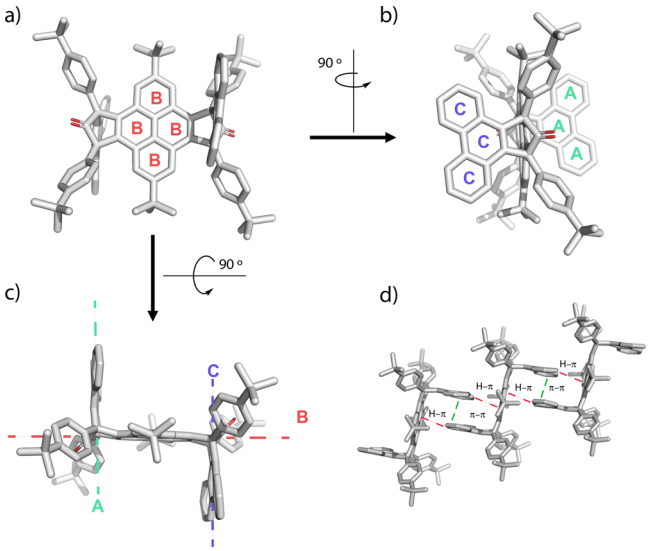

FIGURE 3 | (a–c) Single-crystal structures of **1** from different viewpoints (d) Crystal packing of **1**

methanol into a solution of the compound in toluene (Figure 3). Due to the steric hindrance caused by the bulky substituents, the X-ray structure exhibits a *trans* configuration, which means that the rings constituting the phenanthrene unit (**A** and **C**) are arranged in parallel alternately to each other at a distance of 8.08 Å and forming a 90° angle concerning the central pyrene rings **B** (Figure 3 and Supporting Information, Figure S30).

In addition, we observed the establishment of π interactions between the cores of phenanthrenes (**A** and **C**), simultaneously generating H-π interactions between the hydrogen atoms of phenanthrenes and the central ring of pyrene (Figure 3d, and Supporting Information, Figure S31c, d).

The crystal structure of the **NG1** was isolated and studied, showing the structure presented in Figure 4. The structure of **NG1** was also confirmed by single-crystal X-ray diffraction of the

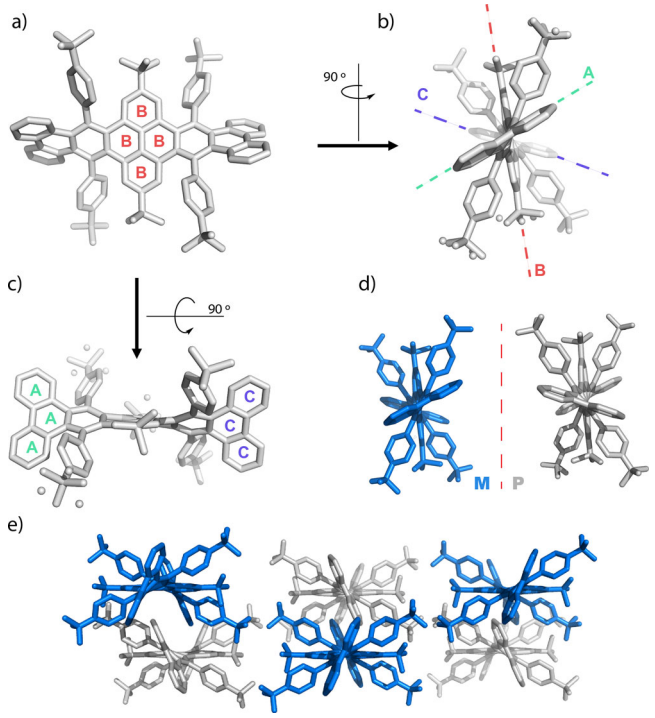

FIGURE 4 | (a–c) Single-crystal structures of **NG1** from different viewpoints. (d) Structure of a pair of enantiomers of **NG1** (e) Crystal packing of **NG1**.

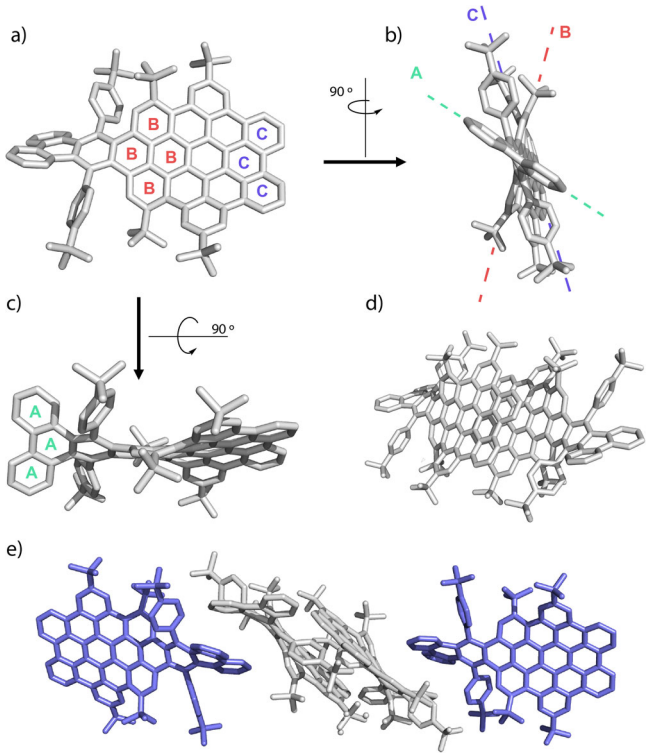

FIGURE 5 | (a–c) Single-crystal structures of **NG2** from different viewpoints. (d) Structure of a pair of enantiomers of **NG2** (e) Crystal packing of **NG2**.

crystals grown by slow diffusion of acetonitrile into a solution of the compound in toluene. The compound has monoclinic symmetry and belongs to the $C_{2/c}$ space group and presents a significant distortion in its structure, due to the incorporation of bulky substituents in the periphery of the acene skeleton (*p-tert*-butylphenyl groups) which increase the H-C_{ar} nonbonded repulsions favoring the twist (Figure 4, a–c). Thus, in such a sterically hindered π system, "the twist" came to disrupt the π-stacking interactions. Even so, the bay region in each extreme of the molecule plays, as well as, an important role in the generation of the torsion if we compare it with the tetracene derivative synthesized by the research group of Mastalerz [38]. The same group, in 2016, isolated a similar hexacene structure, in this case with triptycene in each extreme, but it did not show a twist, even so, a conformer with a twisting angle of 78° was postulated by computational studies [51].

The main moiety of **NG1** is the central pyrene unit (labeled as **B**) that connects the two terminal phenanthrene units, identified as **A** and **C**, respectively. The total length of **NG1** is approximately 17.312 Å, and its height is about 15.533 Å (Figure 4a and b). On one side, the two phenanthrene units (**A** and **C**) are situated in different planes, forming an end- to end torsion angle of 145^0 between them (Figure 4a, b and c). On the other side, each phenanthrene forms an angle of 72^0 with respect to the plane formed by the central pyrene (Figures 4b and Supporting Information, Figures S32 and S34).

These results indicate that the main skeleton of **NG1** does not exhibit optimal planarity. As a consequence of this distortion, **NG1** crystallized in the form of a double helix structure composed of a pair of enantiomers (Figure 4d), exhibiting the self-assembly motif shown in Figure 4e and Supporting Information, Figure S33 showcasing heterochiral packing. Thus, the combination of a substituted central pyrene with two phenanthrene units at the end is an interesting approach to develop and design more stable acenes with potential chiroptical properties.

In addition, the structure of **NG2** was also confirmed by single-crystal X-ray diffraction of the crystals grown by slow diffusion of methanol in a solution of the compound in toluene and CS_2. In comparison with **NG1**, in **NG2** four additional phenylene rings are formed into the HBC core, which significantly alters the geometry of the NG. As a result, the core structure of **NG2** is based on an extended HBC (Figure 5a). On the one hand, the two phenanthrene units (**A** and **C**) lie in distinct planes, defining an end-to-end torsion angle of 132^0 (Figure 5b). On the other hand, the phenanthrene labeled **C** forms an angle of 14.3^0 with respect to the plane of the central pyrene (also labeled **B**), indicating that the HBC core is not completely flat, but exhibits a slight distortion induced by *tert*-butyl groups. These solubilizing groups are arranged alternately above and below the molecular plane (Figures 5a and Supporting Information, Figures S35 and S37). It should be noted that, unlike **NG1**, **NG2** does not crystallize adopting a double helix structure, but presents a homochiral packing characterized by π-π interactions between the HBC cores, located at a distance of 4.75 Å (Figure 5d). On the other hand, the helical part of the acene establishes π-π interactions with the twist portion of the acene belonging to the adjacent molecule, with a distance of 6.70 Å (Figure 5e and Supporting Information, Figure S36).

The resolution of the two enantiomers of each NG was attempted using HPLC and different semi-preparative chiral columns (CHIRALPAK IA/IB). However, despite numerous trials using ternary solvent mixtures, for **NG1**, hexane/THF/IPA (80:19:1) and for **NG2**, hexane/THF/IPA (60:39:1), only two largely overlapping peaks could be observed in the analyses of **NG1** and **NG2**, which prevented any analytical resolution (Supporting Information Figures S38 and S39).

The exceptional solubility of **NG1** and **NG2** in common organic solvents (toluene, THF, and chlorinated solvents) at room temperature is primarily attributed to the distortion present in its skeleton. A fundamental part of understanding the usefulness of prepared NGs is to characterize them in terms of their optoelectronic characteristics. To evaluate these properties and its potencial as organic semiconductor compounds, it is interesting to determine the energies of the HOMO and LUMO orbitals. On one hand, absorption spectroscopy studies of the target compounds provide an estimated value of the optical band gap (E_{gap}^{opt}), taking into account that the lowest energy UV-Vis band corresponds to the HOMO-LUMO monoelectronic excitation. The spectroscopic measurement of **NGs** in toluene at room temperature provided the absorption spectra represented in Figure 6a. In the case of **NG1**, the spectrum presented a band at 350 nm with an extinction coefficient of 97551 $Lmol^{-1}cm^{-1}$ and **NG2** exhibited an extinction coefficient of 101517 $Lmol^{-1}cm^{-1}$ at 407 nm (Figure 6a and Supporting Information, Figure S22). The electronic absorption spectrum of **NG2** appears bathochromically shifted in comparison with **NG1** as a consequence of the extension in the effective conjugation (Figure 6a).

On the other hand, the emission spectra were also investigated in toluene (Figure 6b). Under excitation of the longest wavelength (350 nm for **NG1** and 407 nm for **NG2**), the photoluminescence spectra showed a maxima emission band at 460 nm with a quantum yield of 13.6% for **NG1** and two maxima emission band at 512–550 nm with a quantum yield of 8% for **NG2**. As expected, the emission spectrum of **NG2** also exhibits a bathochromic shift compared to the **NG1** spectrum. This is due to the emission band is originated from the absorption band that is more red-shifted in the spectrum, and therefore, it is a result of the longer extension of the π-system in **NG2**.

The electrochemical properties of NGs were studied by Cyclic Voltammograms (CV) and Square Wave Voltammetry (SWV) in saturated 0.1 M solution of nBu$_4$NPF$_6$ in CH_2Cl_2 using a three-electrode small cell septum, with a glassy carbon disk electrode serving as the working electrode, an Ag reference electrode, and a Pt counter electrode (Figure 6c and Supporting Information, Figure S23). The voltammograms in CH_2Cl_2 reveal an oxidation potential with values of 0.75 and −0.05 V (*vs* Fc/Fc$^+$) for **NG1** and **NG2**, respectively. However, no distinct reduction processes were observed within the solvent-electrolyte window. The oxidation wave is more cathodically shifted and broader in the case of **NG2**, which is consistent with the extended conjugation.

The energy gaps were estimated from the absorption onset of the longest absorption wavelength (Figure 6a). The (E_{gap}^{opt}) of **NG1** and **NG2** were 2.94 and 2.45 eV, respectively. From the onset of the first oxidation wave (Figure 6c and Supporting Information, Figure S23), we could estimate the energy of the HOMO levels as

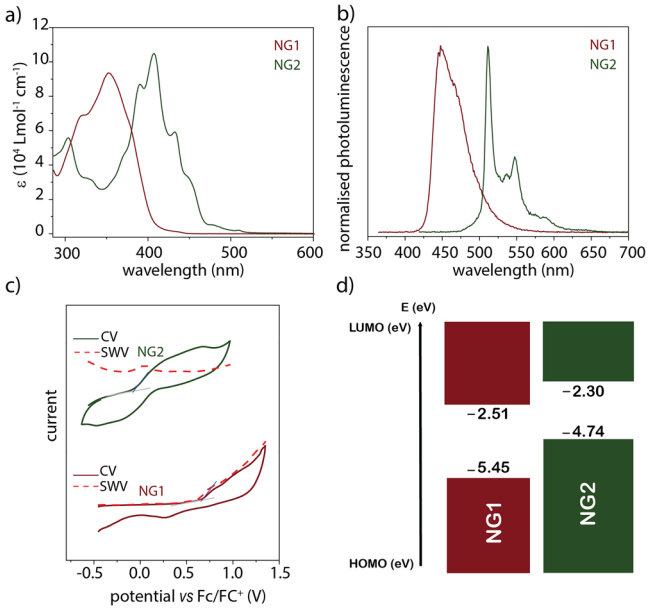

FIGURE 6 | (a) UV-Vis electronic absorption, (b) photoluminescence spectra in toluene (c) Cyclic voltammograms (CV) and Square Wave Voltammetry (SWV) in Ar saturated 0.1 M solution of nBu$_4$NPF$_6$ in CH_2Cl_2. Potential versus Fc/Fc$^+$ of **NG1** and **NG2**. (d) Energy levels of **NG1** and **NG2**.

−5.45 and −4.74 for **NG1** and **NG2**, respectively. Consequently, the LUMO energy levels have been determined from the difference between E_{HOMO} and E_{gap}^{opt} and are −2.51 and −2.30 eV for **NG1** and **NG2**, respectively. The energy gaps are represented in Figure 6d.

We also performed chemical oxidation of NGs using antimony chloride ($SbCl_5$) as an oxidizing agent, monitoring the process using UV-Vis-NIR absorption and ^{1}H NMR spectroscopy. The study began with **NG1** (8.64×10^{-6} M in DCM). After the incremental addition of a $SbCl_5$ solution in DCM (1 M), the light yellow solution of **NG1** turned green, accompanied by the appearance of an absorption band at 500 and 670 nm (green line, Figure 7a). These new signals were assigned to the radical cation (**NG1**$^{\bullet+}$, 290 eq of $SbCl_5$), based on the corresponding theoretical calculations (Supporting Information, Figure S25).

As the amount of $SbCl_5$ was further increased (2300 eq), the solution acquired a red color and a new absorption band appeared in the 500–1100 nm range, with maximum at 520, 720, and 915 nm (red line, Figure 7a). Theoretical calculations confirmed that this new signal corresponded to the dication (**NG1**$^{2+}$, Supporting Information, Figure S25). **NG2** exhibited similar behavior when treated with an excess of $SbCl_5$. In this case, the yellow solution first turned red after the formation of the radical cation (**NG2**$^{\bullet+}$, 1400 eq), with a maximum absorption at 600, 900, and 1300 nm (green line, Figure 7b and Supporting Information, Figure S26). Finally, with the controlled addition of more equivalents of the oxidant, the solution changed to green color, indicating the formation of the dication (**NG2**$^{2+}$, red line, Figure 7b). These experimental results were supported by their theoretical spectra calculations (Supporting Information, Figure S26).

To verify this hypothesis, the chemical titrations were monitored after the addition of the oxidant using ^{1}H NMR spectroscopy. With

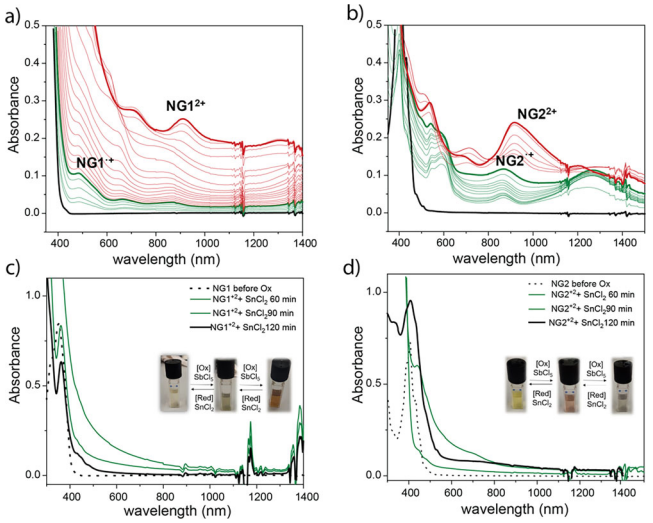

FIGURE 7 | UV-vis spectral changes upon the oxidation of (a) **NG1** (8.64×10^{-6} M in DCM) and (b) **NG2** (1×10^{-5} M in DCM) by incremental addition of $SbCl_5$. UV-vis spectral changes of (c) $NG1^{2+}$ (1×10^{-5} M in DCM/MeCN) and (d) $NG2^{2+}$ in DCM (1×10^{-5} M DCM/MeCN) after the addition of excessive $SnCl_2$ for the indicated time. Inset: Photographs of NGs in DCM observed upon the oxidation by $SbCl_5$ followed with the reduction by $SnCl_2$.

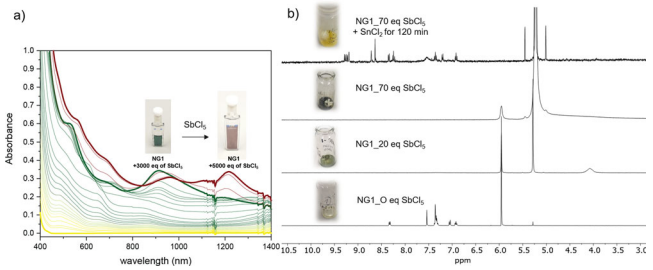

FIGURE 8 | (a) Uv-vis (8.64×10^{-6} M in DCM) and (b) ^{1}H NMR (1×10^{-3} M 400 MHz, $CD_2CD_2Cl_4$ at 25°(c) spectral changes upon the oxidation of **NG1** by incremental addition of $SbCl_5$. (0-5000 eq for UV-vis) and (0-70 eq for ^{1}H NMR spectroscopy).

only 2 equivalents of oxidant (Supporting Information, Figure S27), a marked broadening of the signals was observed, indicating the formation of paramagnetic radical species for **NG1** and **NG2**, respectively.

It is noteworthy that both $\mathbf{NG1}^{2+}$ and $\mathbf{NG2}^{2+}$ could be reversibly reduced to neutral states by adding a solution of tin chloride ($SnCl_2$) in MeCN. During this process, a progressive color change was observed in both NGs. These color changes were accompanied by simultaneous transformations in the UV-Vis-NIR absorption spectra, confirming the complete recovery of the spectrum corresponding to neutral NGs after 120 min of stirring (Figure 7c and d).

Notably, when the amount of $SbCl_5$ equivalents was significantly increased (0-5000 eq for UV-vis and 0–70 eq for ^{1}H NMR spectroscopy), a new absorption band was detected around 1200 nm, accompanied by a change in color to intense red for **NG1** (Figure 8a). Subsequent reduction with $SnCl_2$ produced a

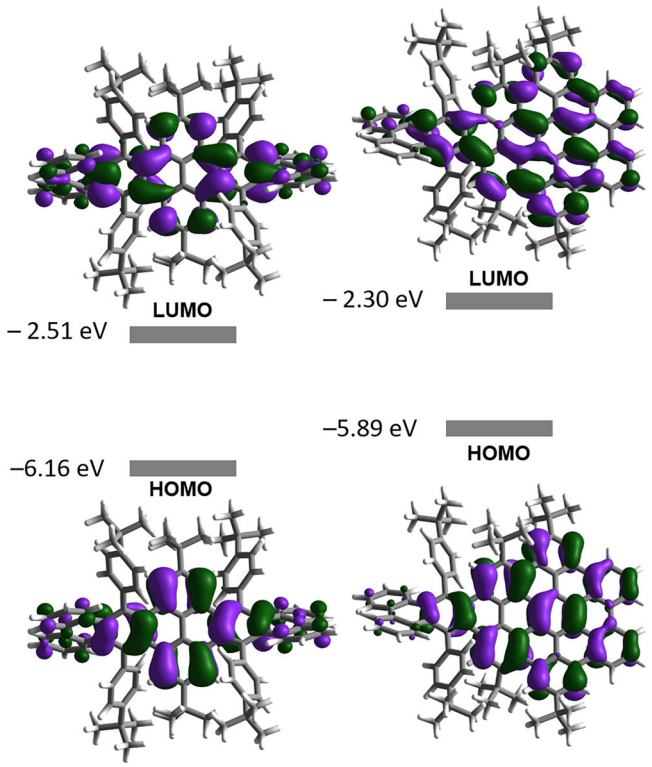

FIGURE 9 | Electronic density of the frontier molecular orbitals of **NG1** and **NG2**.

yellow solid, identified as **NG2** by ^{1}H NMR and MALDI-TOF (Figure 8b and Supporting Information, Figures S28 and S29), confirming that this treatment decisively drives the final stage of the Scholl reaction to a practically quantitative yield, avoiding purification steps and limiting the process to simple filtration [54]. Thus, precise control of the number of $SbCl_5$ equivalents not only allows selective control of the formation of new C–C bonds, but also enables real-time monitoring via UV–Vis–NIR and ^{1}H NMR spectroscopy, whose variations are manifested through color changes, that opens up a versatile synthetic pathway for the design and controlled production of novel NGs.

These experimental results were supported with theoretical computational calculations that has been studied by density functional theory (DFT) and its time-dependent extension (TD-DFT) in CH_2Cl_2 as implemented in Gaussian. Ground state structures were minimized and excited states were computed at CAM-B3LYP/6-31G(d,p) level of theory (Supporting Information, Figure S24). The experimental spectra are in accordance with the TD-DFT calculated electronic transitions, (Supporting Information, Figures S25 and S26). The theoretical calculations also provided information about the energy levels and the electronic distribution of **NG1** and **NG2**. Both molecules show large delocalization along the acene skeleton, including all the rings of the central pyrene (Figure 9). We could compute the energy of the HOMO levels as –6.16 and –5.89 for **NG1** and **NG2**, respectively. However, for a better comparison, the LUMO experimental values were used in the Figure 9, since the LUMO level calculated by DFT is significantly higher than the experimental one, a well-known limitation of Kohn–Sham energy levels [55].

The main orbital transitions and weight contributions to the bright electronic states responsible for the absorption spectra maxima in the UV-vis range of **NG1** and **NG2** are shown in the Supporting Information table S1.

3 | Conclusion

We present the synthesis and characterization of two innovative twistacenes, **NG1** and **NG2**, combining aryne cycloadditions and the Scholl reaction as a synthetic strategy. Most importantly, we have designed a highly efficient synthetic methodology that enables precise control over the selective formation of new C—C bonds during the Scholl reaction. This approach demonstrates the importance of designing NGs with solubilizing groups such as *p-tert*-butylphenyl at specific positions in the aromatic cores, as they facilitate the task of purification and processability of these structures, enabling a broader characterization (^{1}H and ^{13}C NMR, HRMS, UV-vis, photoluminescence, cyclic voltammetry, and square wave voltammetry). Additionally, the single-crystal structures and theoretical calculations revealed a remarkable torsion angle of approximately 145^{0} for **NG1**, positioning it as one of the most notably distorted within the hexacene family and 132^{0} for NG2, being this the first example of a NG that integrates an HBC-containing helical acene fragment. As a result, inducing a significant structural distortion in the resulting architecture of the NG. In addition, this solid-state structures show heterochiral packing for **NG1** and homochiral packing for **NG2** and therefore, serves to verify the correlation between structure and properties. This study provides new application perspectives for helical-twisted NGs that remain practically unexplored in technologies such as next-generation organic solar cells (OSCs) and have emerged as up-and-coming candidates for the design of new organic donor materials.

Acknowledgments

We acknowledge funding from Spanish Agencia Estatal de Investigación (grant number PID2022-140845OB-C62), from the Xunta de Galicia (Centro de Investigacion do Sistema Universitario de Galicia, 2023–2027, grant number ED431G 2023/03), European Research Council Synergy grant MolDAM (grant number 951519), the European Regional Development Fund. The authors acknowledge financial support by the Deutsche Forschungsgemeinschaft (DFG) (Project number 182849149) and Emerging Talents Initiative (ETI) (Project number 2024-2_Nat_05_Mora_Fuentes). The authors thank E. Guitián, H. Maid and C. Placht for fruitful discussions. Deposition Number(s) 2496029 (for **1**), 2496028 (for **NG1**), 2497800 (for **NG2**) contain(s) the supplementary crystallographic data for this paper. These data are provided free of charge by the joint Cambridge Crystallographic Data Centre and Fachinformationszentrum Karlsruhe Access Structures service.

Conflicts of Interest

The authors declare no competing financial interest.

References

1. P. Izquierdo-García, J. M. Fernández-García, and N. Martín, "Twenty Years of Graphene: From Pristine to Chemically Engineered Nano-Sized Flakes," *Journal of the American Chemical Society* 146 (2024): 32222–32234, https://doi.org/10.1021/jacs.4c12819.

2. J. Liu and X. Feng, "Synthetic Tailoring of Graphene Nanostructures With Zigzag-Edged Topologies: Progress and Perspectives," *Angewandte Chemie International Edition* 59 (2020): 23386–23401, https://doi.org/10.1002/anie.202008838.

3. A. Narita, X.-Y. Wang, X. Feng, and K. Müllen, "New Advances in Nanographene Chemistry," *Chemical Society Reviews* 44 (2015): 6616–6643, https://doi.org/10.1039/C5CS00183H.

4. W. Klemm, "Metalloids and Their Compounds With the Alkali Metals," *Proceedings of the Chemical Society* (1958): 329–364, https://doi.org/10.1039/PS9580000329.

5. E. Clar, C. T. Ironside, and M. Zander, "28. The Electronic Interaction Between Benzenoid Rings in Condensed Aromatic Hydrocarbons. 1: 12-2: 3-4: 5-6: 7-8: 9-10: 11-Hexabenzocoronene, 1: 2-3: 4-5: 6-10: 11-tetrabenzoanthanthrene, and 4: 5-6: 7-11: 12-13: 14-Tetrabenzoperopyrene," *Journal of the Chemical Society (Resumed)* 28 (1959): 142, https://doi.org/10.1039/jr9590000142.

6. A. Halleux, R. H. Martin, and G. S. D. King, "Synthèses dans la série des dérivés Polycycliques Aromatiques Hautement Condensés. L'hexabenzo-1,12; 2,3; 4,5; 6,7; 8,9; 10,11-coronène, le tétrabenzo-4,5; 6,7; 11,12; 13,14-péropyrène et le tétrabenzo-1,2; 3,4; 8,9; 10,11-bisanthène," *Helvetica Chimica Acta* 41 (1958): 1177–1183, https://doi.org/10.1002/hlca.19580410502.

7. W. Hendel, Z. H. Khan, and W. Schmidt, "Hexa-peri-Benzocoronene, A Candidate for the Origin of the Diffuse Interstellar Visible Absorption Bands ?," *Tetrahedron* 42 (1986): 1127–1134, https://doi.org/10.1016/S0040-4020(01)87517-7.

8. V. S. Iyer, M. Wehmeier, J. D. Brand, M. A. Keegstra, and K. Müllen, "From Hexa- peri -hexabenzocoronene to "Superacenes"," *Angewandte Chemie International Edition in English* 36 (1997): 1604–1607, https://doi.org/10.1002/anie.199716041.

9. H. Arslan, F. J. Uribe-Romo, B. J. Smith, and W. R. Dichtel, "Accessing extended and partially fused hexabenzocoronenes using a benzannulation–cyclodehydrogenation approach," *Chemical Science* 4 (2013): 3973, https://doi.org/10.1039/C3SC51212F.

10. Y. Zhang, S. H. Pun, and Q. Miao, "The Scholl Reaction as a Powerful Tool for Synthesis of Curved Polycyclic Aromatics," *Chemical Reviews* 122 (2022): 14554–14593, https://doi.org/10.1021/acs.chemrev.2c00186.

11. M. Müller, C. Kübel, and K. Müllen, "Giant Polycyclic Aromatic Hydrocarbons," *Chemistry—A European Journal* 4 (1998): 2099–2109, https://doi.org/10.1002/(SICI)1521-3765(19981102)4:11⟨2099::AID-CHEM2099⟩3.0.CO;2-T.

12. I. Pozo, E. Guitián, D. Pérez, and D. Peña, "Synthesis of Nanographenes, Starphenes, and Sterically Congested Polyarenes by Aryne Cyclotrimerization," *Accounts of Chemical Research* 52 (2019): 2472–2481, https://doi.org/10.1021/acs.accounts.9b00269.

13. H. Ito, K. Ozaki, and K. Itami, "Annulative π-Extension (APEX): Rapid Access to Fused Arenes, Heteroarenes, and Nanographenes," *Angewandte Chemie International Edition* 56 (2017): 11144–11164, https://doi.org/10.1002/anie.201701058.

14. D. Lungerich, O. Papaianina, M. Feofanov, et al., "Dehydrative π-extension to Nanographenes With Zig-zag Edges," *Nature Communications* 9 (2018): 4756, https://doi.org/10.1038/s41467-018-07095-z.

15. S. Ma, J. Gu, C. Lin, Z. Luo, Y. Zhu, and J. Wang, "Supertwistacene: A Helical Graphene Nanoribbon," *Journal of the American Chemical Society* 142 (2020): 16887–16893, https://doi.org/10.1021/jacs.0c08555.

16. J. Liu, B.-W. Li, Y.-Z. Tan, et al., "Toward Cove-Edged Low Band Gap Graphene Nanoribbons," *Journal of the American Chemical Society* 137 (2015): 6097–6103, https://doi.org/10.1021/jacs.5b03017.

17. R. Zuzak, I. Pozo, M. Engelund, et al., "Synthesis and Reactivity of a Trigonal Porous Nanographene on a Gold Surface," *Chemical Science* 10 (2019): 10143–10148, https://doi.org/10.1039/C9SC03404H.

18. S. R. Peurifoy, Q. Xu, R. May, et al., "Air-stable, Long-length, Solution-based Graphene Nanoribbons," *Chemical Science* 11 (2020): 9978–9982, https://doi.org/10.1039/D0SC02105A.

19. S. T. Bao, Y. Hong, H. Jiang, et al., "Chirality Unbound in Graphene Nanoribbons," *Angewandte Chemie International Edition* 64 (2025): e202508426, https://doi.org/10.1002/anie.202508426.

20. N. Wang, K. Zhao, T. Ding, et al., "Improving Interfacial Charge Recombination in Planar Heterojunction Perovskite Photovoltaics With Small Molecule as Electron Transport Layer," *Advanced Energy Materials* 7 (2017): 1700522, https://doi.org/10.1002/aenm.201700522.

21. X. Wang, L. Chen, L. Wang, et al., "Synthesis of Novel Nanomaterials and Their Application in Efficient Removal of Radionuclides," *Science China Chemistry* 62 (2019): 933–967, https://doi.org/10.1007/s11426-019-9492-4.

22. X.-Y. Yan, M.-D. Lin, S.-T. Zheng, et al., "Recent Advances of Hexaazatriphenylene (HAT) Derivatives: Their Applications in Self-Assembly and Porous Organic Materials," *Tetrahedron Letters* 59 (2018): 592–604, https://doi.org/10.1016/j.tetlet.2018.01.004.

23. J. L. Segura, R. Juárez, M. Ramos, and C. Seoane, "Hexaazatriphenylene (HAT) Derivatives: From Synthesis to Molecular Design, Self-Organization and Device Applications," *Chemical Society Reviews* 44 (2015): 6850–6885, https://doi.org/10.1039/C5CS00181A.

24. T. Wöhrle, I. Wurzbach, J. Kirres, et al., "Discotic Liquid Crystals," *Chemical Reviews* 116 (2016): 1139–1241, https://doi.org/10.1021/acs.chemrev.5b00190.

25. R. Rieger and K. Müllen, "Forever Young: Polycyclic Aromatic Hydrocarbons as Model Cases for Structural and Optical Studies," *Journal of Physical Organic Chemistry* 23 (2010): 315–325, https://doi.org/10.1002/poc.1644.

26. S. Hauptmann, "The Aromatic Sextet: Von E in Seiten mit Zahlreichen Formelbildern; Format 13 ×20 cm; Broschiert £1, 50 Zeitschrift für," *Chemie* (1972): 200–200, https://doi.org/10.1002/zfch.19730130531.

27. A. Borissov, Y. K. Maurya, L. Moshniaha, W.-S. Wong, M. Żyła-Karwowska, and M. Stępień, "Recent Advances in Heterocyclic Nanographenes and Other Polycyclic Heteroaromatic Compounds," *Chemical Reviews* 122 (2022): 565–788, https://doi.org/10.1021/acs.chemrev.1c00449.

28. D. Cortizo-Lacalle, J. P. Mora-Fuentes, K. Strutyński, A. Saeki, M. Melle-Franco, and A. Mateo-Alonso, "Monodisperse N-Doped Graphene Nanoribbons Reaching 7.7 Nanometers in Length," *Angewandte Chemie International Edition* 57 (2018): 703–708, https://doi.org/10.1002/anie.201710467.

29. R. A. Pascal, "Twisted Acenes," *Chemical Reviews* 106 (2006): 4809–4819, https://doi.org/10.1021/cr0505501.

30. R. G. Clevenger, B. Kumar, E. M. Menuey, and K. V. Kilway, "Synthesis and Structure of a Longitudinally Twisted Hexacene," *Chemistry—A European Journal* 24 (2018): 3113–3116, https://doi.org/10.1002/chem.201705676.

31. R. A. Pascal Jr., W. D. McMillan, D. Van Engen, and R. G. Eason, "Synthesis and Structure of Longitudinally Twisted Polycyclic Aromatic Hydrocarbons," *Journal of the American Chemical Society* 109 (1987): 4660–4665, https://doi.org/10.1021/ja00249a032.

32. R. G. Clevenger, B. Kumar, E. M. Menuey, G.-H. Lee, D. Patterson, and K. V. Kilway, "A Superior Synthesis of Longitudinally Twisted Acenes," *Chemistry—A European Journal* 24 (2018): 243–250, https://doi.org/10.1002/chem.201704501.

33. W. Fan, T. Winands, N. L. Doltsinis, Y. Li, and Z. Wang, "A Decatwistacene With an Overall 170° Torsion," *Angewandte Chemie International Edition* 56 (2017): 15373–15377, https://doi.org/10.1002/anie.201709342.

34. J. Xiao, H. M. Duong, Y. Liu, et al., "Synthesis and Structure Characterization of a Stable Nonatwistacene," *Angewandte Chemie International Edition* 51 (2012): 6094–6098, https://doi.org/10.1002/anie.201200949.

35. W. Chen, X. Li, G. Long, et al., "Pyrene-Containing Twistarene: Twelve Benzene Rings Fused in a Row," *Angewandte Chemie International Edition* 57 (2018): 13555–13559, https://doi.org/10.1002/anie.201808779.

36. J. Lu, D. M. Ho, N. J. Vogelaar, et al., "Synthesis, Structure, and Resolution of Exceptionally Twisted Pentacenes," *Journal of the American Chemical Society* 128 (2006): 17043–17050, https://doi.org/10.1021/ja065935f.

37. H. I. Yuuta Yano, Y. Segawa, and K. Itami, "Helically Twisted Tetracene: Synthesis, Crystal Structure, and Photophysical Properties of Hexabenzo[a,c,fg,j,l,op]Tetracene," *Synlett* 27 (2016): 2081–2084, https://doi.org/10.1055/s-0035-1561455.

38. K. B. Sven, M. Elbert, J. A. Esteves, L. Weber, F. Rominger, and M. Mastalerz, "Pyrene-Based Diarynes as Precursors for Twisted Fused Polycyclic Aromatic Hydrocarbons: A Comparison of Two Routes," *Organic Materials* 02 (2020): 358–361, https://doi.org/10.1055/s-0040-1721851.

39. R. K. Dubey, M. Melle-Franco, and A. Mateo-Alonso, "Inducing Single-Handed Helicity in a Twisted Molecular Nanoribbon," *Journal of the American Chemical Society* 144 (2022): 2765–2774, https://doi.org/10.1021/jacs.1c12385.

40. A. Swain, K. Radacki, H. Braunschweig, and P. Ravat, "Helically Twisted Nanoribbons via Stereospecific Annulative π-Extension Reaction Employing [7]helicene as a Molecular Wrench," *Chemical Science* 15 (2024): 11737–11747, https://doi.org/10.1039/D4SC01814A.

41. J. M. Fernández-García, P. Izquierdo-García, M. Buendía, S. Filippone, and N. Martín, "Synthetic Chiral Molecular Nanographenes: The Key Figure of the Racemization Barrier," *Chemical Communication* 58 (2022): 2634–2645, https://doi.org/10.1039/D1CC06561K.

42. S. Míguez-Lago, I. F. A. Mariz, M. A. Medel, et al., "Highly Contorted Superhelicene Hits Near-Infrared Circularly Polarized Luminescence," *Chemical Science* 13 (2022): 10267–10272, https://doi.org/10.1039/D2SC03452B.

43. C. M. Cruz, S. Castro-Fernández, E. Maçôas, J. M. Cuerva, and A. G. Campaña, "Undecabenzo[7]Superhelicene: A Helical Nanographene Ribbon as a Circularly Polarized Luminescence Emitter," *Angewandte Chemie International Edition* 57 (2018): 14782–14786, https://doi.org/10.1002/anie.201808178.

44. M. Buendía, J. M. Fernández-García, J. Perles, S. Filippone, and N. Martín, "Enantioselective Synthesis of a Two-fold Inherently Chiral Molecular Nanographene," *Nature Synthesis* 3 (2024): 545–553, https://doi.org/10.1038/s44160-024-00484-x.

45. P. Izquierdo-García, J. M. Fernández-García, J. Perles, and N. Martín, "Enantiomerically Pure Helical Bilayer Nanographenes: A Straightforward Chemical Approach," *Journal of the American Chemical Society* 146 (2024): 34943–34949, https://doi.org/10.1021/jacs.4c14544.

46. S. Marcos López, M. Buendia, I. Fernández, S. Filippone, and N. Martín, "A Diastereoselective Scholl Reaction: Point-to-helical Chirality Transfer in Molecular Nanographenes," *Chemical Science* 16 (2025): 12867–12872, https://doi.org/10.1039/D5SC02563J.

47. D. Di Nuzzo, C. Kulkarni, B. Zhao, et al., "High Circular Polarization of Electroluminescence Achieved via Self-Assembly of a Light-Emitting Chiral Conjugated Polymer into Multidomain Cholesteric Films," *ACS Nano* 11 (2017): 12713–12722, https://doi.org/10.1021/acsnano.7b07390.

48. M. Li, S.-H. Li, D. Zhang, et al., "Stable Enantiomers Displaying Thermally Activated Delayed Fluorescence: Efficient OLEDs With Circularly Polarized Electroluminescence," *Angewandte Chemie International Edition* 57 (2018): 2889–2893, https://doi.org/10.1002/anie.201800198.

49. D.-W. Zhang, M. Li, and C.-F. Chen, "Recent Advances in Circularly Polarized Electroluminescence Based on Organic Light-Emitting Diodes," *Chemical Society Reviews* 49 (2020): 1331–1343, https://doi.org/10.1039/C9CS00680J.

50. J. R. Brandt, F. Salerno, and M. J. Fuchter, "The Added Value of Small-molecule Chirality in Technological Applications," *Nature Reviews Chemistry* 1 (2017): 0045, https://doi.org/10.1038/s41570-017-0045.

51. K. Baumgärtner, A. L. Meza Chincha, A. Dreuw, F. Rominger, and M. Mastalerz, "A Conformationally Stable Contorted Hexabenzoovalene," *Angewandte Chemie International Edition* 55 (2016): 15594–15598, https://doi.org/10.1002/anie.201607740.

52. D. Rodríguez-Lojo, D. Peña, D. Pérez, and E. Guitián, "Aryne-mediated Syntheses of Structurally Related Acene Derivatives," *Organic & Biomolecular Chemistry* 8 (2010): 3386, https://doi.org/10.1039/c003422n.

53. Y. Byun, M. Cho, D. Kim, Y. Jung, and A. Coskun, "Edge-Functionalized Graphene Nanoribbon Frameworks for the Capture and Separation of Greenhouse Gases," *Macromolecules* 50 (2017): 523–533, https://doi.org/10.1021/acs.macromol.6b02483.

54. B. Xiao, Z.-J. Liu, B.-Q. Wang, P. Hu, C. Redshaw, and K.-Q. Zhao, "Synthesis of Triphenylene Discotic Liquid Crystals Possessing Nine Alkyl Chains: Influence of Molecular Symmetry and Chain Length on Mesomorphism," *Molecular Crystals and Liquid Crystals* 577 (2013): 25–35, https://doi.org/10.1080/15421406.2013.781489.

55. G. Zhang and C. B. Musgrave, "Comparison of DFT Methods for Molecular Orbital Eigenvalue Calculations," *The Journal of Physical Chemistry A* 111 (2007): 1554–1561, https://doi.org/10.1021/jp061633o.

Supporting Information

Additional supporting information can be found online in the Supporting Information section.

Supporting file: chem70712-sup-0001-SuppMat.docx